

## Puzzling Frequencies in First Overtone Cepheids

W. A. Dziembowski

Warsaw University Observatory, Al. Ujazdowskie 4, 00-478 Warsaw, Poland  
Copernicus Astronomical Center, ul. Bartycka 18, 00-716 Warsaw Poland  
e-mail: wd@astrouw.edu.pl

*Received October 3, 2012*

### ABSTRACT

The OGLE project led to discovery of earlier unknown forms of multiperiodic pulsation in Cepheids. Often, the observed periods may be explained in terms of simultaneous excitation of two or rarely three radial modes. However, a secondary variability at about 0.6 of the dominant period, detected in a number of the first overtone (1O) pulsators inhabiting the Magellanic Clouds, seems to require a different explanation. After reviewing a possibility of explaining this signal in terms of radial and nonradial modes, I find that only unstable modes that may reproduce the observed period ratio are f-modes of high angular degrees ( $\ell = 42-50$ ). I discuss in detail the driving effect behind the instability and show that it is not the familiar opacity mechanism. Finally, I emphasize the main difficulty of this explanation, which requires high intrinsic amplitudes implying large broadening of spectral line.

**Key words:** *Galaxies: Magellanic Clouds Stars: variables: Cepheids Stars: oscillations*

### 1. Introduction

When a secondary periodicity is detected in a Cepheid, the initial hypothesis is always that this is due to excitation of another radial mode. There are some theoretical and observational arguments against interpretation in terms of nonradial modes. None of the arguments is compelling, especially if the amplitude of the secondary variability is low. However, the interpretation in terms of radial mode is the most attractive because only then the secondary periodicity yields immediately a precise constraint on stellar parameters. The strength of information contained in data on two radial mode periods is best seen in the impact of the seminal Petersen's (1973) paper on stellar physics. The huge mass discrepancy revealed in the diagram  $P_S/P_L$  vs.  $\log P_L$  known as the Petersen diagram prompted the major stellar opacity revision. Such diagrams are still commonly used to confront data with models.

In 1973 the list of double-mode Cepheid contained 8 objects. The number of such objects has been considerably increased thanks to massive photometry of stars in the Magellanic Clouds within the framework of the microlensing projects: MA-CHO, OGLE, and EROS. In particular, the OGLE-III Catalog of Cepheids in the

LMC lists 61 objects pulsating simultaneously in fundamental and first overtone modes (F/1O), and 203 in two consecutive overtones (1O/2O). Similar numbers (F/1O – 59, 1O/2O – 215) of double mode Cepheids are listed in the catalog for the SMC (Soszyński *et al.* 2008). The catalog contains also some rare objects with frequencies which may be interpreted in terms of different combinations of radial modes. Exceptionally valuable are objects where three radial modes are identified. Data on the three periods allow for an independent determination of the distance to Magellanic Clouds (Moskalik and Dziembowski 2005). With a precisely determined distance, massive photometry yields strong constraints on models of individual double-mode Cepheids.

In a number of Cepheids, the period of the secondary variability is incompatible with the radial mode interpretation. First such cases were discovered by Moskalik and Kołaczkowski (2008, 2009) in their analysis of OGLE-II data for the LMC. They found such periods in 42 objects with dominant mode being first overtone and named them FO- $\nu$  Cepheids. In most of the cases the secondary periods were close to the dominant modes and were interpreted as an analogue of the Blazkho effect in RR Lyr stars. However, in 7 objects, the secondary periods were between 0.6 and 0.64 of the dominant (first overtone) period and required a different interpretation. After rejecting the possibility that the secondary periodicity is associated with another radial mode, the authors concluded that the high-frequency signal is due to a nonradial modes but noted the problem with driving such modes. The difficulties of this interpretation were also briefly discussed by Dziembowski and Smolec (2009). It is interesting that though the Cepheid masses ( $1\text{--}2 M_{\odot}$ ) determined by Petersen (1973) were by at least by a factor of 3 lower than accepted at his time, still interpretations other than simultaneous excitation of F and 1O modes were never considered in published papers.

The subsequent phase of the OGLE project led to the discovery of many more Cepheids with the dominant first overtone and the period ratio in the 0.6–0.64 range. The OGLE-III Catalog provides data on 29 objects of this type in the LMC and 139 in the SMC. They seem most puzzling Cepheids posing interesting questions. First of all we would like to know what is the nature of the secondary periodicity. We also would like to understand why they are so much more frequent in the SMC than in the LMC and why there is apparently no counterpart of this phenomenon among Cepheids pulsating in the fundamental mode.

In Section 2 I review the data and reconsider the two-radial mode interpretation, taking into account data on periods and reddening-free magnitudes. On the model side, linear instability of considered modes is set as the requirement. Interpretation of the secondary periodicity in terms of nonradial mode excitation is studied in Section 3. Section 4 is devoted to explanation of driving mechanism acting in various modes. Visibility of high-degree modes which reproduce the whole range of puzzling frequencies is discussed in Section 5.

## 2. The 1O/X Cepheids in the Magellanic Clouds

### 2.1. The LMC

The difficulty of the two-radial mode interpretation for the 1O-X Cepheids in the LMC is demonstrated in Fig. 1. The data shown there are from Soszyński *et al.* (2008) and they include in addition to the two periods, the Wesenheit index, which is a reddening-free stellar luminosity measure evaluated from mean  $I$  and  $V$  magnitudes with the standard expression

$$W_I = I - 1.55(V - I). \quad (1)$$

The envelope models and radial pulsation periods were calculated with the standard Warsaw codes (see, *e.g.*, Moskalik and Dziembowski 2005) for stellar parameters leading to unstable 1O modes in the period range of the 1O/X pulsators. Two sets of abundance parameters were adopted  $(Z, Y) = (0.008, 0.256)$  and  $(0.004, 0.24)$ , which are most often used for modeling young stars in the LMC and SMC, respectively. For each selected value of  $Z$ ,  $M$  (mass in solar units), and  $L$  (luminosity in solar units) two values of the effective temperatures were selected. The higher one corresponding to the onset of the 1O instability defines blue edge (BE). The one by 0.04 dex lower was adopted as the red edge (RE) of the considered ranges of  $T_{\text{eff}}$ . With our code we cannot determine the red edge. The choice of 0.04 is in a crude agreement with results of nonlinear modeling of Cepheid pulsation with time-dependent versions of the Mixing Length Theory (MLT, Feuchtinger *et al.* 2000) and the observed range of the  $V - I$  color (see Fig. 3).

The MLT parameter  $\alpha = 1.5$  was adopted for this plot but the value of  $\alpha$  has only marginal influence on calculated periods. The growth rates are more affected. With  $\alpha = 0.5$ , BE and RE are shifted by about  $-0,015$  dex. An increase of  $\alpha$  above 1.5 does extend the instability range of the third overtone but even at  $\alpha = 2.5$  this modes remains stable in the relevant range of stellar parameters. The ranges of luminosity were chosen to cover the whole range of  $\log P_{1O}$ . Models used in this plots are realistic in the sense of physics but do not follow from stellar evolution calculations. In fact, at the considered  $Z$  values no such calculation predicts entering the instability strip at  $M = 3$  in the He burning phase. At  $M = 4$  some do but only models that include overshooting reach  $\log L > 3$  in this phase.

In the upper panel of Fig. 1, we may see that the objects split into two nearly equinumerous groups with period ratios in the  $[0.599, 0.607]$  and  $[0.619, 0.627]$  ranges. The objects occur in a rather narrow period range, extending from 0.24 to 0.41 days. One of these objects (shown with the encircled symbol) is an F/1O pulsator. The  $P_{1O}/P_{FO} = 0.714$  ratio at  $\log P_F = 0.506$  is well within the range of F/1O Cepheids in LMC but the  $A_F/A_{1O} = 0.04$  is exceptionally low. There is nothing that significantly distinguishes this object from the rest in Fig. 1.

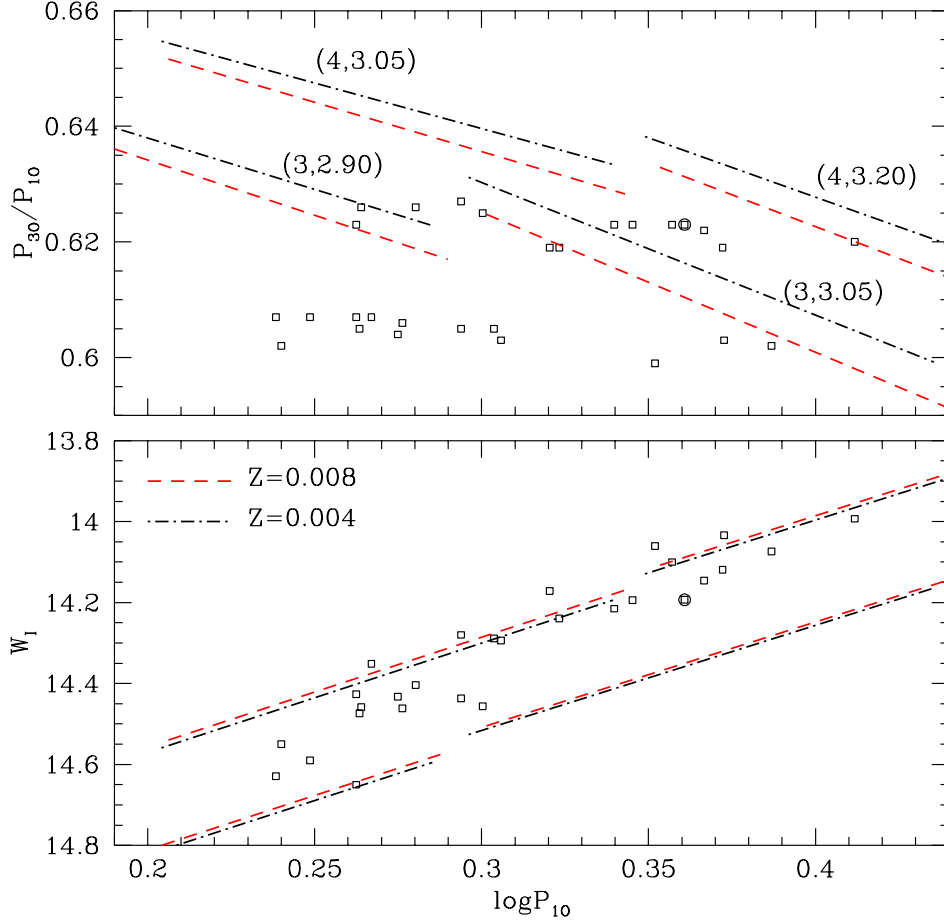


Fig. 1. Comparison of the periods and the  $W_I$  luminosity indices for the 1O/X Cepheids in the LMC from the OGLE-III catalog with model values. Observational data are shown with symbols. The encircled symbol in *both panels* refers to the object where the fundamental radial mode is excited along with the first overtone. The *upper panel* shows Petersen diagram. The symbols are based on the measured  $P_{10}$  and  $P_X$  periods. The calculated periods refer to the first and third overtones in the envelope models with two indicated metal abundance parameters,  $Z$ , shown with lines. Individual lines cover the range of  $T_{\text{eff}}$  of the first overtone instability strip (see text for explanation), at specified mass,  $M$ , and luminosity,  $L$ . The values of  $M$  and  $\log L$ , expressed in solar units, are given above each pair of the lines. The *lower panel* shows the period-luminosity relation employing the Wesenheit luminosity index,  $W_I$ , (see Eq. 1).

There is no doubt regarding 1O identification of the dominant mode. The only radial mode that may be contemplated for association with  $P_X$  is 3O because for realistic stellar models  $P_{20}/P_{10} \gtrsim 0.77$  and  $P_{40}/P_{10} \lesssim 0.55$  in the range of  $P_{10}$  shown in Fig 1. At specified  $P_{10}$  the  $P_{30}/P_{10}$  ratio depends both on  $Z$  and  $M$ . To disentangle two effect we need data on luminosity.

The model values of  $W_I$  shown in the bottom panel were calculated with the bolometric corrections and color indices are taken from Kurucz (2004) assuming

the 18.5 mag distance modulus to LMC. We see in the lower panel that the dependence on  $Z$  is very weak and that models of the same mass lie nearly on a single line in the  $\log P_{10}-W_I$  diagram. Thus, the position in this diagram is a rather clean probe of stellar mass. We see that the majority of the 1O/X Cepheids in the LMC have masses close to 4. Only at short periods they are significantly lower but higher than 3. At  $M \approx 4$  the plots in the upper panel leave the possibility of the O3 interpretation for the secondary mode only for one object, which is near  $\log P_{10} = 0.4$ . Some of the data are reproduced by models with  $M \approx 3$  but these are inconsistent with positions in the lower panel. In many cases the fit requires  $M$  significantly lower than 3. An independent argument against the 3O identification for the secondary mode comes from stability calculations which show that in all considered models this mode is stable. Thus, even for the object at  $\log P_{10} \approx 0.4$  such identification is excluded. In fact, it is the most distant from the instability range.

## 2.2. The SMC

There are nearly five times as many 1O/X Cepheids in the SMC than in the LMC and, as we may see in Fig. 2, the range of  $\log P_{10}$  where the objects occur is by a similar factor wider. The lack of objects with  $\log P_{10} < 0.2$  in the LMC may be explained by much smaller total number of the 1O Cepheids in this galaxy (see Fig. 9 of Soszyński *et al.* 2010). However, even at longer periods, the number of the 1O/X is by a factor of 2.4 larger though, beginning with  $\log P_{10} = 0.3$ , the number of 1O Cepheid in the LMC is greater than in the SMC. The differences in the incidence of the 1O/X Cepheids between the two clouds are striking. In this paper we focus mainly on the SMC data because much larger population reveals the pattern which for the less numerous LMC objects may not be visible.

Table 1

Three sequences of 1O Cepheids: mean parameters and standard deviations

sequence	$P_X/P_{10}$	$\log P_{10}$	$W_I$	$V-I$	No
A	$0.610 \pm 0.003$	$0.106 \pm 0.071$	$15.54 \pm 0.27$	$0.56 \pm 0.06$	65
B	$0.623 \pm 0.002$	$0.297 \pm 0.066$	$14.90 \pm 0.30$	$0.61 \pm 0.05$	50
C	$0.638 \pm 0.003$	$0.443 \pm 0.065$	$14.37 \pm 0.25$	$0.65 \pm 0.04$	24

There are three well-detached sequences of 1O/X Cepheids concentrated around  $P_X/P_{10} = 0.610$ , 0.623, and 0.638 marked in Fig. 2 as A, B, and C, respectively. These ratios are correlated with periods but there is some overlap. Within each of the sequence we see a slow decline of the period ratio with  $P_{10}$ . The mean parameters of stars forming the three sequences are listed in Table 1. Only the objects in sequence B have their counterparts in the LMC. The objects in sequence A, except of one, occur at much shorter periods than the LMC objects with similar period

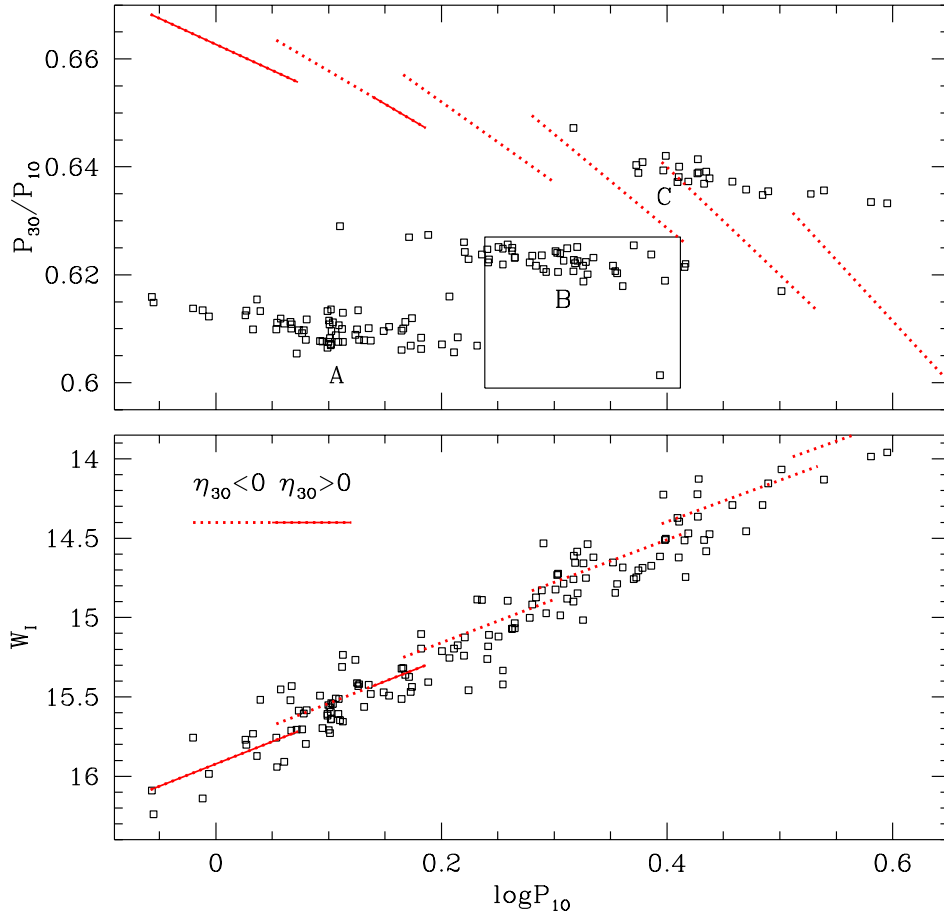


Fig. 2. Comparison of the periods and the  $W_1$  luminosity indexes for the OGLE-III data (Soszyński *et al.* 2010) for the 10/X Cepheids in the SMC with model values. Models used in this plot were calculated assuming  $Z = 0.004$ , and the  $M-L$  relation given in Eq. (2). Each of the six lines extends over the O1 instability strip (as defined in the text) at fixed  $L$  and  $M$ . In the part shown in the solid style also O3 modes are unstable. The adopted range of  $\log L$ , is  $[2.7, 3.45]$  and the resulting range of  $M$  is  $[3.2, 5.17]$ . The rectangle in the *upper panel* shows the range of the 10/X Cepheids in the LMC.

ratios. There are no 10/X Cepheids in the OGLE-III data for the LMC with the period ratio as high as found in sequence C. It should be stressed, however, that Moskalik and Kołaczowski (2009) in their analysis of the OGLE-II data detected three such objects.

The color–magnitude and period–magnitude diagrams depicted in Fig. 3 show that the 10/X pulsators occur over nearly whole range of parameters of the first overtone Cepheids in the SMC except that they are absent at shortest periods. There are 320 first overtone Cepheids at  $\log P_{10} < 0.056$  but in none of them the puzzling high frequency signal has been detected although the incidence of the 10/X pulsators in the whole population is about 8.5%. This, in part, may be blamed to difficulty of detecting this low amplitude signal in fainter objects but is unlikely to

account for the whole effect.

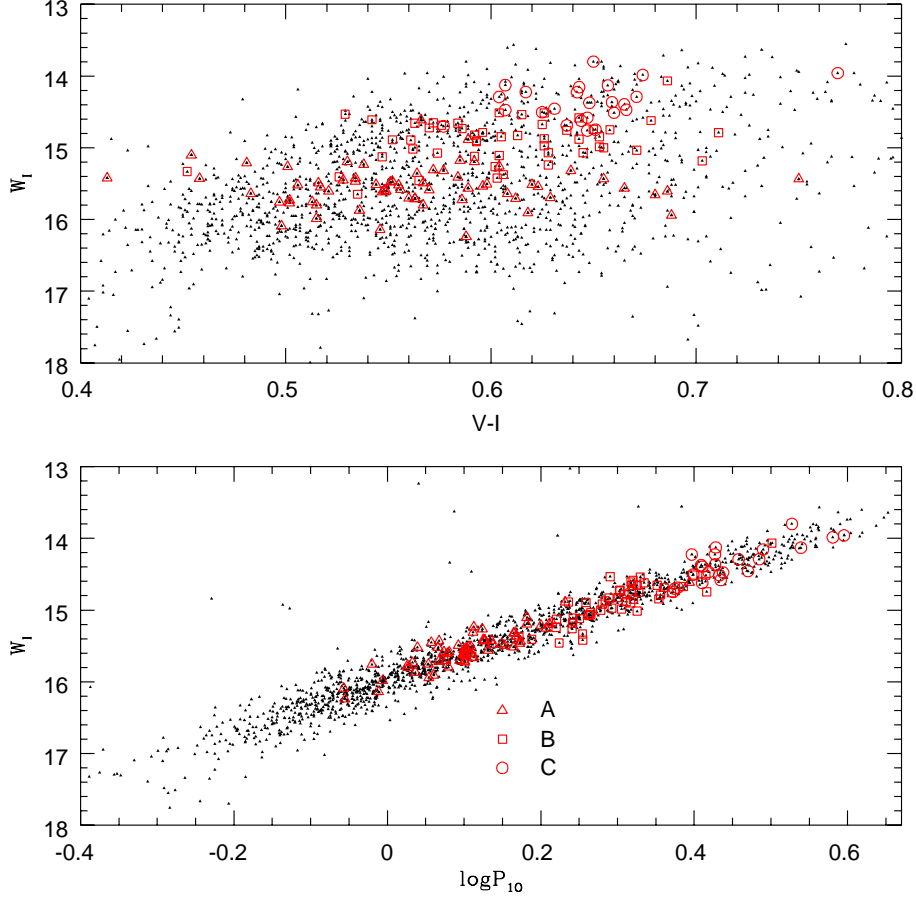


Fig. 3. The 10 Cepheids in SMC from OGLE-III catalog in the CM and PL diagram. The 10/X objects from the three sequences are marked with different symbols.

Models used for comparison with the data in Fig. 2 satisfy the mass–luminosity relation

$$\log L = 3.05 + 3.6(\log M - 0.602), \quad (2)$$

which is based on Girardi *et al.* (2000) evolutionary models of stars with masses  $M = 4$  and  $5$  at  $Z = 0.004$ . The tracks with  $M = 3$  do not reach the instability strip in the helium burning phase. BaSTI (Pietrinferni *et al.* 2006) models also at  $M = 4$  and  $5$  do not reach the instability strip but the maximum values of  $L$  in this evolutionary phase is in a good agreement with the relation given by Eq. (2). Similar conclusion was reached by Smolec (private communication), who used public domain code MESA (Paxton *et al.* 2011). Apparently, new evolutionary codes do not describe well the Cepheid phase. In the lower panel of Fig. 2, we may see that with the adopted mass–luminosity relation the observational data in the  $P_{10} - W_I$

plane are well reproduced. Interestingly, I found it also for the LMC data. Models calculated with  $Z = 0.008$ , which have lower  $M$  at the same  $L$ , produce lines running well above observational data. This suggests that the occurrence of 1O/X pulsation requires low metal abundance and perhaps in this way may explain the large difference in the incidence of such a pulsation form between the two systems.

### 2.3. Problems with Two Radial Modes Hypothesis

The problem with reconciling the secondary period with  $P_{30}$  for the SMC 1O/X Cepheid is different at short and long periods. In the first case, it is the large discrepancy in the period ratios and in the second it is the stability of the third overtone. It is not easy to find modification of stellar structure resulting in the required change in the period ratios. Any admissible changes in  $Z$  cannot do it. A factor of  $\sim 10$  increase suffices to get agreement for the sequence B but not for sequence A. The plots in Fig. 3 do not reveal any anomaly that would suggest nonstandard models for the 1O/X Cepheids. The absence of these objects in the short period range, which presumably is populated by stars crossing the instability strip, may suggest that the occurrence of the secondary periodicity is related to some property of the deep interior structure. One conceivable feature affecting mainly frequencies of higher overtones could be a composition jump at fractional mass above  $M_r/M \approx 0.6$  but it is not expected in the relevant stellar models.

The stability problem may seem less severe because the determination of the instability ranges suffers from the poor understanding of interaction between convection and pulsation. However, especially for sequence C objects, we are far from the period range where the third overtone is unstable. This is seen not only in results of calculations but also in the observational data. There is one object in the SMC at  $\log P_{10} \approx -0.65$ , that is, well below Fig. 2 range where almost certainly the third overtone is excited together with the first two overtones (see Fig. 4 in Soszyński *et al.* 2010). In the LMC there are three O1/O2/O3 Cepheids all located near  $\log P_{10} = -0.25$  (see Fig. 2 in Soszyński *et al.* 2008). Again this is far from the 1O/X range.

Perhaps the correct interpretation of the 1O/X Cepheids requires going beyond the linear pulsation theory. However, since the period ratios are significantly different from the ratios of low integers, the only possibility seems to be a modification of the mean stellar structure by the 1O presence leading to a modification of 3O properties. This possibility remains to be studied.

## 3. Nonradial Modes and the Puzzling Frequencies

The problem with nonradial mode excitation in giants is the strong damping in the radiative interior which is a consequence of huge values of the Brunt-Väisälä frequency, hence very large radial wave numbers. However as Osaki (1977) first showed there is a class of nonradial modes that despite strong damping in the core



are unstable owing to the same driving effect as radial modes. The instability occurs if the modes are sufficiently well trapped in the envelope and this is possible if the angular degree is sufficiently high. In the  $7 M_{\odot}$  Cepheid model, the instability started at  $\ell = 4$  and the period close to 10 and at  $\ell = 6$  and the period close to the fundamental radial mode. Frequencies and growth rates were determined for envelope models alone upon assuming the running wave inner boundary condition. At the same time, I found (Dziembowski 1977) similar unstable modes in RR Lyr models. Formal derivation of the inner boundary is given in that paper. There is one-to-one correspondence between trapped nonradial and radial modes, thus following earlier habits, we will use names f- and p<sub>n</sub>-modes. In particular, the 10 mode corresponds to p<sub>1</sub> nonradial modes, all having one node in the acoustic cavity.

Thirty years later, Mulet-Marquis *et al.* (2007) revisited the problem. They conducted an extensive survey relying on complete stellar models and their advanced tools for solving equations for nonradial oscillations. All numerical results presented in the present paper were obtained with the same code I developed over 35 years ago. A comparison with modern results shows that this is adequate. We all share the same major uncertainty, that is, the treatment of convection.

Fig. 5 depicts the relative driving rates

$$\eta = \frac{\int d^3\mathbf{x}w}{\int d^3\mathbf{x}|w|} \quad (3)$$

where

$$w = \Im \left[ \delta P \left( \frac{\delta \rho}{\rho} \right)^* \right]$$

is the local contribution to the work integral, for selected models of Cepheid envelopes. The value of  $\eta$  varies between  $-1$  (no driving zone) and  $1$  (no damping zone). This parameter, which was introduced by Stellingwerf (1978), is a better measure of the instability strength than the usual growth rates and also better predictors for the nonlinear development.

Only in the cooler (RE) model at the lowest  $L$  do we find unstable low degree modes. Unstable are p<sub>3</sub>-modes at  $\ell = 3, 4, 5$ . At  $\ell = 5$  the period is significantly shorter than  $P_{30}$  and the period ratio is not far from that found in sequence A objects but the instability is marginal. At lower degrees periods are very close to  $P_{10}$ . In any of the models considered by us, not only those used in Fig. 4, the p-mode instability range does not extend much beyond  $P_{30}$  if this mode is unstable. The f-modes are clearly different. They are strongly unstable. The maximum of  $\eta$  occurs in the observed range of  $P_X/P_{10}$  but there is a difficulty following from high angular degrees, which in this range are between  $\ell = 40$  and  $50$ . Thus, large pulsation amplitudes are needed to offset effect of cancellation in the mean variability. We will return to this difficulty in Section 6. Let us first try to explain why f-mode driving is so efficient.

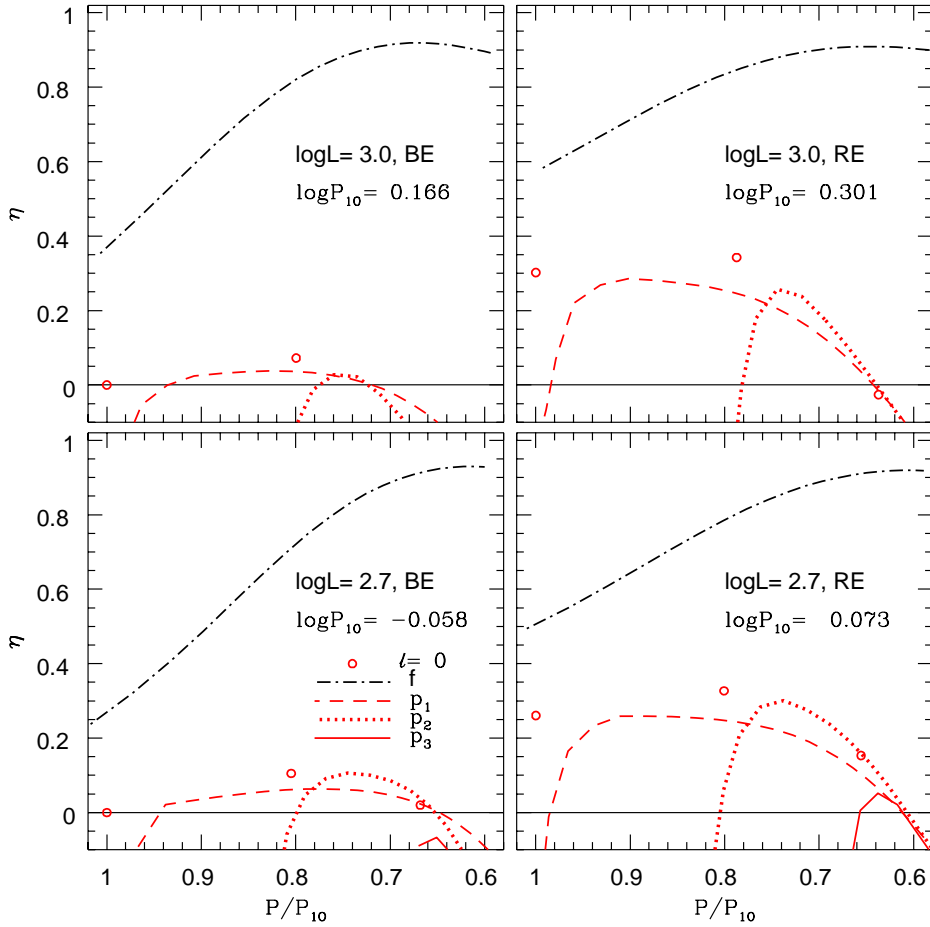


Fig. 4. The relative driving rate for trapped acoustic modes and high-degree f-modes in selected models ( $M = 3.2$  at  $\log L = 2.7$  and  $3.87$  at  $\log L = 3.0$ ). In the  $\log L = 2.7$  BE (the 10 blue edge) model the  $\ell$ -ranges of unstable  $p_1$  and  $p_2$  modes are  $[6,21]$  and  $[4,10]$ , respectively. In the cooler model (RE) at the same luminosity the corresponding  $\ell$ -ranges are  $[5,22]$ , and  $[3,12]$ . In this model there are unstable  $p_3$ -modes at  $\ell = 3, 4$ , and  $5$ . In the  $\log L = 3$  BE, model the ranges are  $[7,15]$ , and  $[5,6]$  while in the  $\log L = 3$  RE model, the ranges are  $[4,19]$ , and  $[4,9]$ . In all models the f-mode shown have  $\ell$  ranging from 16 to 54 but the instability extends well beyond this range.

#### 4. The Driving Mechanism behind the f-Mode Instability

That high-degree modes are unstable over wide range of stellar parameters has been known since long time ago (Dziembowski 1977, Shibahshi and Osaki 1981). The authors of both papers noted the instability extends beyond the blue edge for radial pulsation and that the hydrogen ionization is the main site of the driving effect but they failed to explain the driving mechanism. My aim in this section is to supply the explanation.

Let us focus on two models with the same parameters at the surface but differing in the efficiency of the convective transport. Plots in Fig. 5 and 6 refer to models

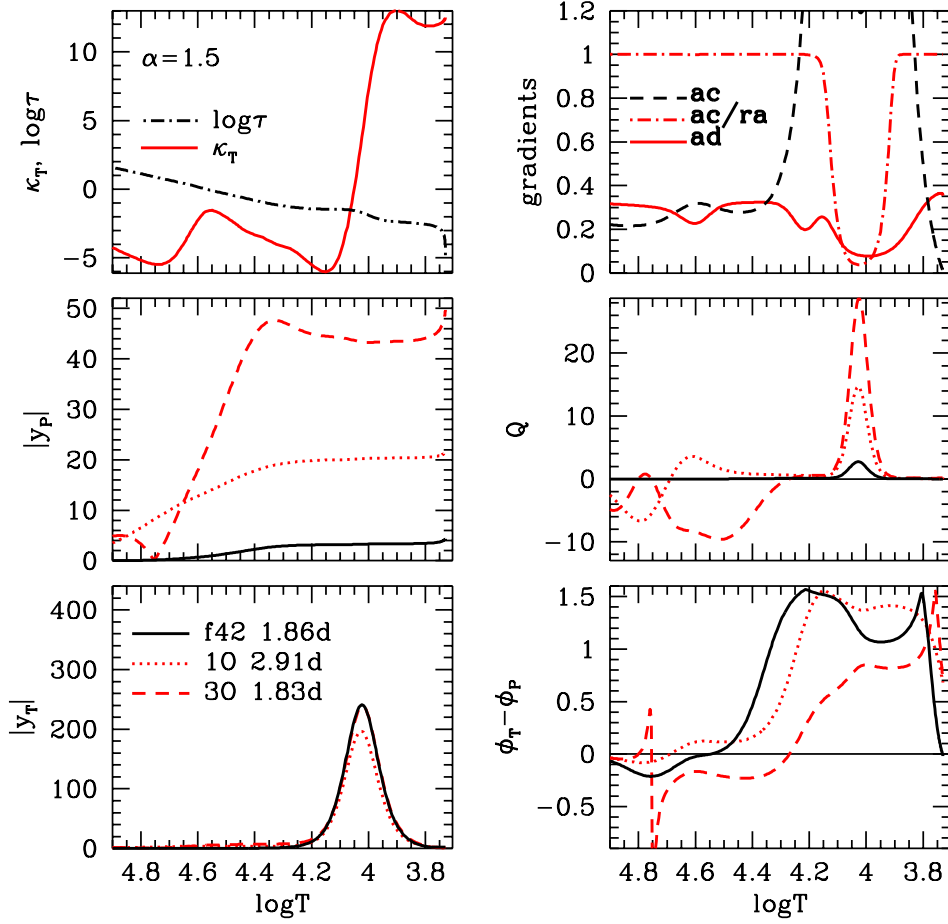


Fig. 5. Plotted against the local temperature in outer layers are various quantities relevant for understanding driving and damping effects working in the three selected modes. The model is characterized by the global parameters  $M = 4.69$ ,  $\log L = 3.3$ , and  $\log T_{\text{eff}} = 3.806$ . It was calculated assuming the mixing length parameter  $\alpha = 1.5$ . The selected modes are 1O and 3O radial modes and the  $\ell = 42$  f-mode (f42). Their periods are listed in the *left bottom panel*. The *top left panel* shows the opacity derivative  $\kappa_T = (\partial \log \kappa / \partial \log T)_P$  and the thermal time scale in days,  $\tau$  of the envelope above each point. The *upper right panel* shows the actual temperature in the envelope  $d \ln T / d \ln P \equiv \nabla$ , the ratio of actual to radiative gradient,  $\nabla / \nabla_{\text{rad}}$ , and the adiabatic gradient  $\nabla_{\text{ad}}$ . The *middle and panels on the left-hand side* show the absolute values of the radial eigenfunctions for the pressure and temperature perturbation, respectively. The *bottom right panel* shows the phase difference between the two eigenfunctions. Plotted in the *middle right panel*  $Q$  (see Eq. 4) is the local contribution to driving per unit of the independent variable.

calculated with  $\alpha = 1.5$  and  $0.5$ , respectively. The choice of  $\alpha$  has a significant effect on nonadiabatic mode properties. In particular, the relative driving rates for the O1, O3, and  $\ell = 42$  f-mode (f42) are, respectively  $0.29$ ,  $-0.65$ , and  $0.87$  at  $\alpha = 1.5$ , while at  $\alpha = 0.5$  the corresponding rates are  $0.04$ ,  $-0.99$ , and  $0.93$ . However, the huge difference in  $\eta$ , between O3 and f42 is preserved and this is true for all models considered in this paper. This may look like a paradox. These

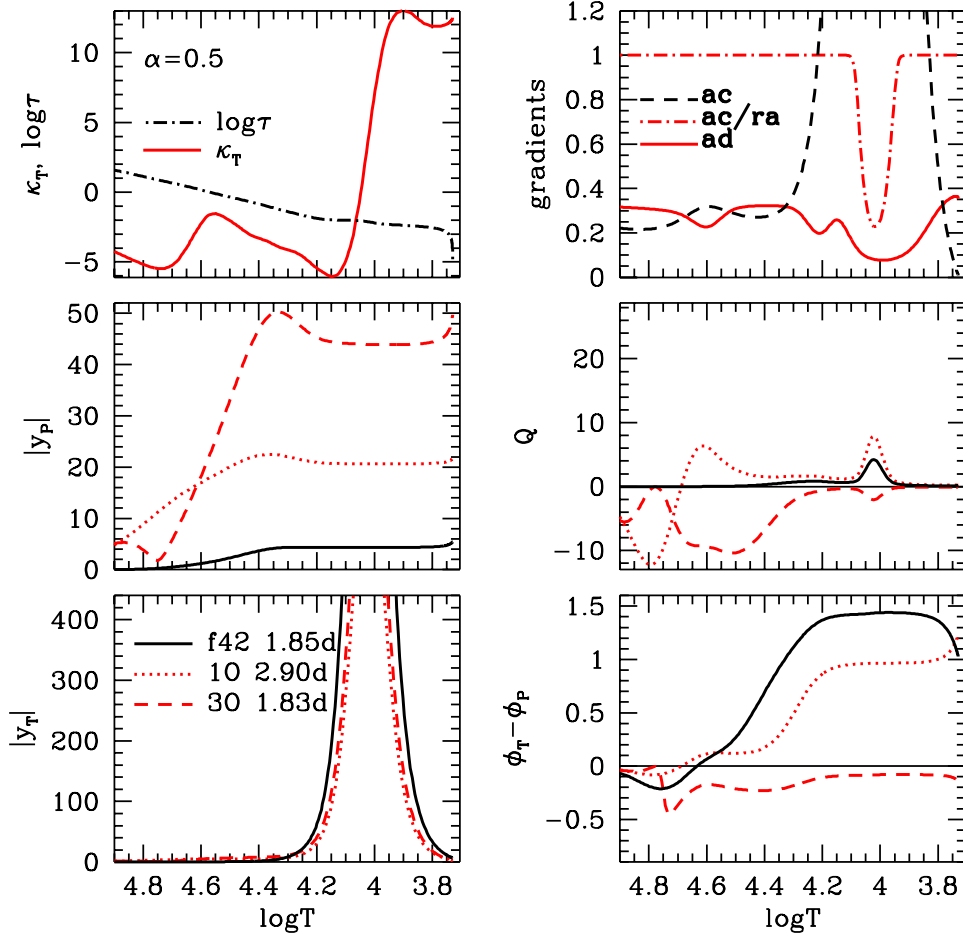


Fig. 6. Same as Fig. 5 but for models calculated with  $\alpha = 0.5$  instead of 1.5.

two modes have nearly the same periods; there is an additional energy loss in f42 resulting from the horizontal radiative flux and yet this mode is driven in nearly the whole outer part of the star where it is trapped. In Figs. 5 and 6 the driving layers may be recognized as places where  $Q > 0$ . This quantity is proportional to  $w$  (see Eq. 3) and it is given by

$$Q = Q_N \frac{Pr^3}{\nabla V} \left( -\frac{\partial \log \rho}{\partial \log T} \right)_p \mathfrak{I}(y_P^* y_T) \quad (4)$$

where  $Q_N$  is the normalization constant, which is the same for all modes in Figs. 5 and 6,  $V = -d \log P / d \log r$ , while  $y_P(r)$  and  $y_T(r)$  are radial eigenfunctions corresponding to  $\delta P / P$  and  $\delta T / T$ . The angular and time dependence of perturbations is assumed in the form  $Y_\ell^m \exp(-i\omega t)$ . The standard normalization  $y_r = 1$  at the surface was adopted for the radial eigenfunctions. In Figs. 5 and 6 in addition to  $Q$ , plotted are  $|y_P|$ ,  $|y_T|$ , and the phase difference  $\phi_T - \phi_P$ , whose sign sets the sign

of  $Q$ .

The classical opacity mechanism acts only in the HeII ionization zone and only in 1O. Note rising  $\kappa_T$  between  $\log T = 4.7$  and 4.55 and the associated bump of  $Q$  for this mode. For O3 this is the damping zone because its amplitude varies rapidly and the radiative losses dominate. Convection is present in this zone but carries a negligible fraction of energy, even at  $\alpha = 1.5$ . In the layers above the thermal time-scale is much shorter than periods of the modes. Thus pulsation becomes very nonadiabatic. The common feature of the modes is steep peak of  $|y_T|$  centered at  $\log T \approx 4.05$ . Its height depends on mode and  $\alpha$  but neither on its localization nor its shape. In certain range around its maximum,  $|y_T|$  is roughly determined by the equation

$$\frac{dy_T}{d\log T} = 2.3(\kappa_T - 4)y_T + C \quad (5)$$

where  $C$ , which includes all remaining terms from the expression for perturbed radial component of the radiative flux, is regarded constant. Associated with the  $|y_T|$  peak is the peak of  $Q$  at the same location, except for 3O at  $\alpha = 0.5$  when we see there a deep. Always higher  $\alpha$  enhances driving effect in radial overtones and it is opposite to f-modes, where higher  $\alpha$  results in some reduction of  $\eta$ . Apparently, in the latter case the effect of increased  $|y_T|$  dominates over the effect of increased  $\tau$ . Regardless of the value of  $\alpha$  the phase difference does not change much in the layer around the  $|y_T|$  maximum. Its growth takes place below, between  $\log T = 4.6$  and 4.2. Thus, the driving mechanism actually works there and not in layers around maximum of  $Q$ .

In order to identify the effect causing instability of the high-degree f-modes, we transform the expression for  $Q$  (Eq. 4) using

$$\Im \left( \frac{\delta P^*}{P} \frac{\delta T}{T} \right) = \Im \left( \frac{\delta P^*}{P} \frac{\delta S}{c_P} \right) = \frac{1}{c_P} \Re \left[ \frac{\delta P^*}{\omega P} \delta(\nabla \mathbf{F}) \right]$$

where  $\mathbf{F}$  denotes the total energy flux per unit area. Then, we separate  $Q$  into the part arising from the vertical ( $Q_V$ ) and horizontal ( $Q_H$ ) part of  $\delta(\nabla \mathbf{F})$ . Adopting the convective flux freezing approximation in the form  $\delta(r^2 F_{\text{conv}}) = 0$ , we obtain

$$Q_V = \frac{Q_N L \nabla_{\text{ad}}}{4\pi} \Re \left( \frac{y_P^*}{\omega} \frac{dy_F}{d \ln T} \right), \quad (6)$$

$y_F$  is the radial eigenfunction corresponding to  $\delta(4\pi r^2 F_{\text{rad}})/L$ , and

$$Q_H = -\frac{Q_N L \nabla_{\text{ad}}}{4\pi} \frac{\ell(\ell+1)}{\nabla \nabla_{\text{rad}} V^2} \Re \left( \frac{y_P^*}{\omega} (y_T + y_r \nabla V) \right). \quad (7)$$

The two contributions and the net value of  $Q$  in the f42 mode are plotted in Fig. 7, where we may see that below  $\log T = 4.2$  the horizontal energy losses lead to pulsation energy gain ( $Q_H > 0$ ). In order to understand why is it so let us note

that  $(y_T + y_r \nabla V)$  is the radial eigenfunction for the relative Eulerian perturbation of temperature,  $T'/T$ . If  $\omega$  is regarded real, which is not far from true, we have  $Q_H \propto \Re(\delta P * T')$ . Thus, driving takes place if cooling, which is proportional to  $T'$ , occurs in the low pressure phase and heating occurs in the high pressure phase, just like in the well-known case of semi-convective instability in the presence of the mean molecular weight gradient. Long-time ago Souffrin and Spiegel (1967) found that the same effect may cause instability of the gravity waves also in chemically homogeneous layers. In the present situation,  $Q_H > 0$  because in the considered range of  $\log T$ , the advection term  $y_r \nabla V$  dominates in  $T'$  and the phase difference  $\psi_r - \psi_P \approx \pi/2$  is largely fixed by the inner boundary condition.

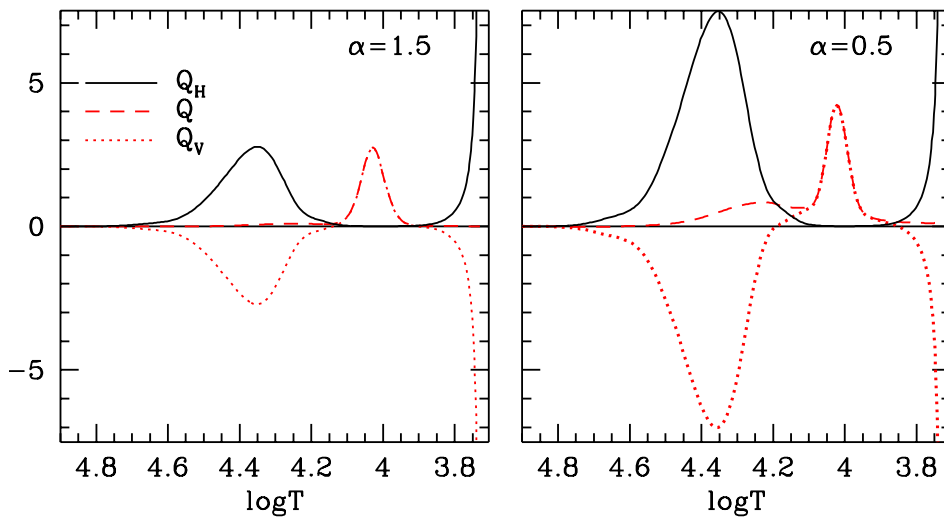


Fig. 7. Values of  $Q_V$  and  $Q_H$  in models used in Figs. 1 and 2.

The pulsation energy gain from  $Q_H > 0$  is nearly canceled out by  $Q_V < 0$  because we are in the region where  $\tau \ll P_X$  and thus there is a tendency toward the temporal thermal equilibrium. This changes near  $\log T = 4.2$ , where the steep rise of opacity inhibits the horizontal diffusion and creates the  $y_T$  bump, which enhances the vertical diffusion. Most of the contribution to driving arises there but the essential phase lag  $\psi_T - \psi_P$  is created below.

## 5. Visibility of High Degree Modes

We have noted in Section 3 that the f-modes that could explain the Petersen diagram for the 10/X Cepheid must have rather high degrees. The plots in the upper panel of Fig. 8 suggest the  $\ell = 42, 46,$  and  $52$  are excited in sequence A, B, and C, respectively. The fact that only even degree modes are seen is consistent with expectations because cancellation causes more rapid decline of the disc-averaged amplitudes for odd-degree modes but why multiples of four are preferred is difficult

to explain. The  $p_1$  modes in the same frequency range have  $\ell$ 's by about a factor of 2 lower, hence they might appear a better option for the identification. However, the  $\ell$ -values best fitting for the three sequences are odd (19, 21, and 23) hence are disfavored by the visibility argument. The arguments discussed already in Section 4 also speaks against the  $p_1$  option. In the RE models, the unstable  $p_1$  at  $\ell = 19$  occur only for  $\log P_{10} \lesssim 0.3$ , at  $\ell = 21$  for  $\log P_{10} \lesssim 0.1$ , and at  $\ell = 23$  for  $\log P_{10} \lesssim 0$ , hence to the left of the great majority of the data point. In the BE models the instability ranges are still narrower. They are also narrower in models calculated with lower  $\alpha$ .

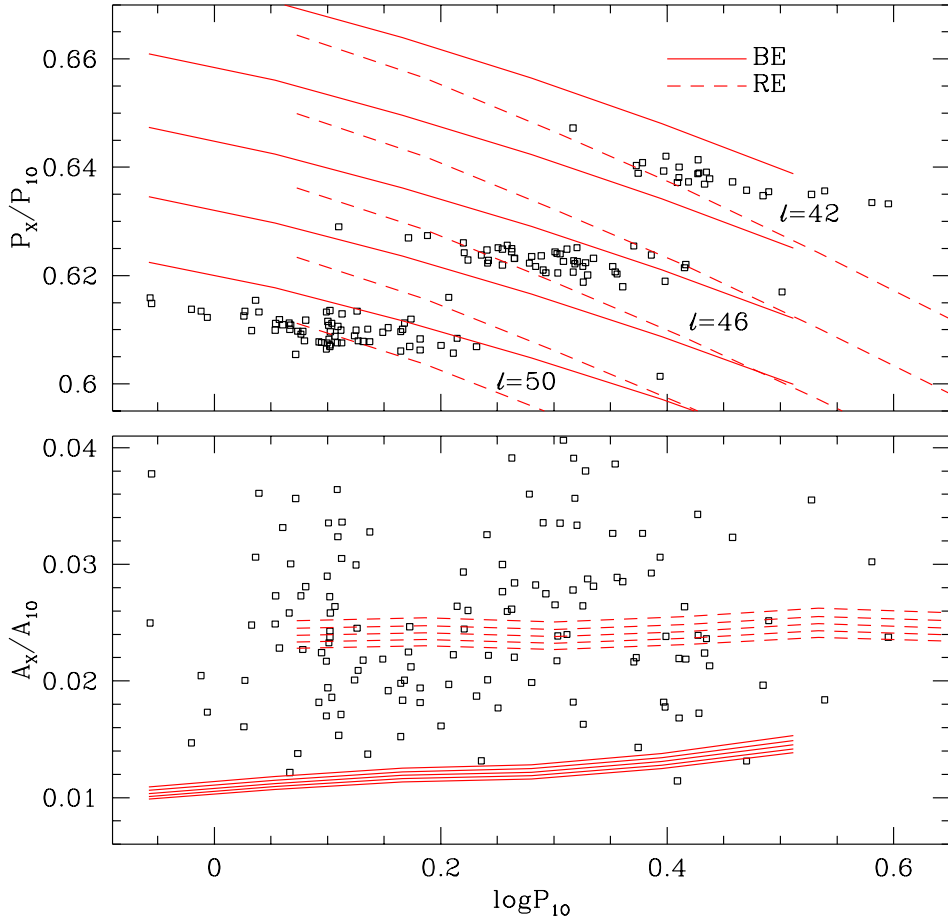


Fig. 8. In the *upper panel*, the  $P_X/P_{10}$  period ratio for the 10-X Cepheids are compared with the evaluated ratios of  $P_\ell/P_{10}$  at even  $\ell$ 's for the same models as used in Fig. 2. The labels showing mode degrees are put between the lines corresponding to the red and blue edges of the instability strip. In the *lower panel*, the observed amplitude ratios in the  $I$ -band are compared with calculated amplitudes assuming the same intrinsic amplitudes for the  $f$ -modes and the 10 mode.

The calculated amplitude ratios shown in the lower panel were obtained assuming the same rms amplitudes of the photospheric radius variations,  $\overline{\delta R}_{\text{rms}}$ , for all

modes. The numbers were obtained with the use of parameters from Kurucz (2004) models and Claret (2000) description of the limb-darkening law. The disc-averaged fluxes were evaluated with help of the recurrence relation following Townsend (2003). The observable amplitudes of the f-modes decrease slowly with  $\ell$  because in this range the dominant cause of the light changes is the geometrical distortion. With the parabolic limb-darkening law, the amplitude is proportional to  $\ell^{-0.5}$  if  $\ell$  is even. The decline is also slow with the Claret version. Much larger ratios for the RE than BE models follow primarily from much larger surface values of  $y_F$  for the 1O mode.

The comparison with observations suggests that  $\overline{\delta R_{\text{rms}}}$  amplitudes of the f-modes would have to be of the same order as that of the 1O mode to explain the 1O/X Cepheids. This is a very crude conclusion because it is based on the linear relation between the flux and radius amplitudes whereas at such intrinsic amplitudes we are then well beyond validity of the linear approximation. We should also keep in mind that calculated values refer to aspect-averaged amplitudes while the actual amplitudes depend on aspect angle,  $i$ , and on the mode azimuthal order,  $m$ , which we do not know. Certainly, the high intrinsic amplitudes of the nonradial modes required for this interpretation is a serious difficulty. However, with interpretation in terms of the  $p_1$  modes, we get the amplitude ratios lower only by some 50%. Taking into account the other difficulties of this hypothesis discussed earlier, we cannot regard it as a viable alternative.

The difficulty of the interpretation in terms of the high- $\ell$  f-modes is best revealed with the estimate of the radial velocity variations within stellar photosphere,

$$v_{\text{rad}}(\theta, \phi, t) = \frac{A_v}{2} \Re \left[ \left( Y_\ell^m \cos i - \frac{1}{\ell} \frac{\partial Y_\ell^m}{\partial \theta} \sin i \right) \exp(-i\omega t) \right],$$

with  $A_v = 2\omega \overline{\delta R_{\text{rms}}}$ . This expression uses  $\omega^2 = \ell GMR^{-3}$ , which is approximately valid for these modes. The value of  $\overline{\delta R_{\text{rms}}}$  may be expressed in terms of the aspect-average light amplitude. Keeping only the contribution from geometrical distortion of the stellar surface, we get

$$\frac{A_v}{A_I} = 0.047 \frac{R}{P_{1O}} \left[ \ell(\ell+1) \int_0^1 h_I(\mu) \mu d\mu \right]^{-1} \quad [\text{km/s/mmag}] \quad (8)$$

where the photospheric radius,  $R$ , is expressed in the solar units and  $P_{1O}$  in days, while  $h(\mu)$  describes the limb-darkening law. This quantity, evaluated for the same models as used in Fig. 2, is shown in the lower panel of Fig. 9. To estimate the local radial velocity we may use data on light amplitude, which are plotted in the upper panel. The typical velocity amplitudes range from 35 km/s for sequence C to 70 km/s for sequence A. These are very large numbers. At so high  $\ell$ 's, the expected signature is a nearly constant spectral line broadening. Such large effect could not be overlooked. Unusually broad line profiles ( $\Delta\lambda/\lambda > 10^{-4}$ ) were observed in certain galactic Cepheids. Kovtyukh *et al.* (2003), report such a phenomenon in



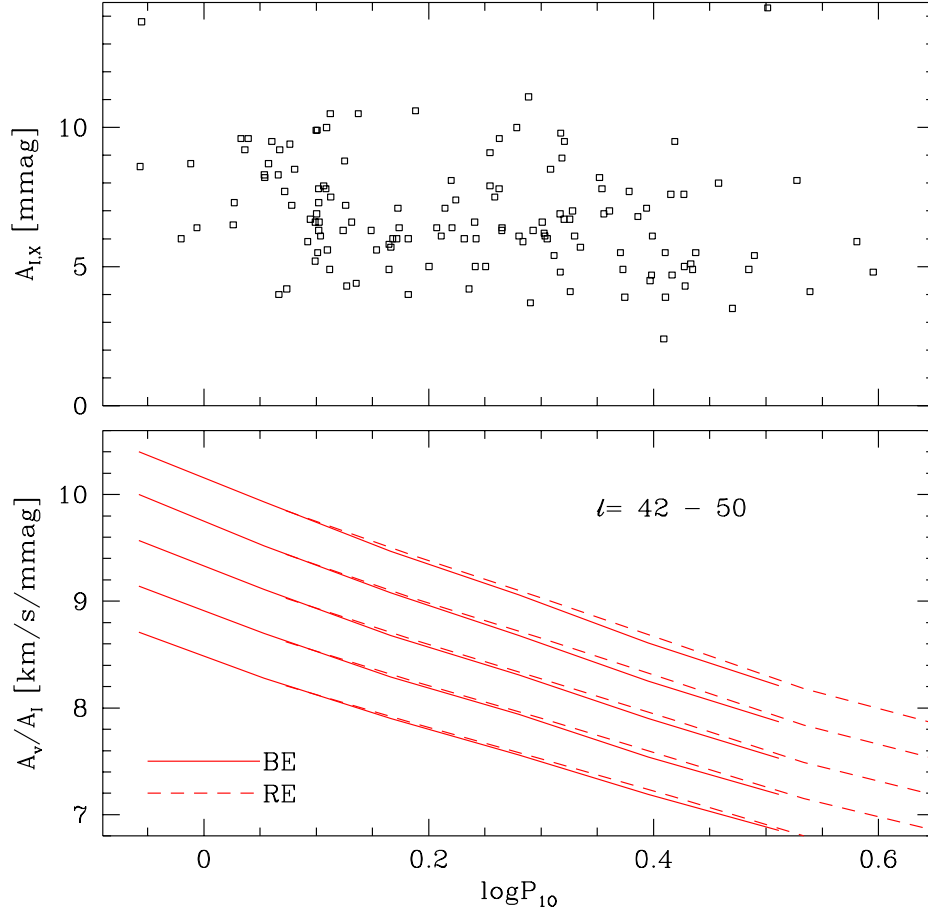


Fig. 9. The *upper panel* shows the full light amplitude in the *I*-band determined for the 10-X Cepheids. The amplitude ratio plotted in *lower panel* was evaluated with the use of Eq. (8) for same models as used in Fig. 8.

four objects, of which three are certainly and one is possibly first overtone pulsator. The authors noted significant changes in the line profiles during pulsation cycle including moving bumps. Their cautious interpretation is that low degree nonradial modes are excited in these stars. Indeed, the observed patterns suggest rather low  $\ell$ 's.

The high degree mode instability is found over the whole luminosity range of the classical instability strip and its blueward extension (Dziembowski 1977, Shibahashi and Osaki 1981). In all the cases the dominant contribution to excitation arises in the hydrogen ionization zone. The direct evidence that such modes are indeed seen in stars comes from observations of the line profile variations in  $\delta$  Sct stars. In particular, Kennelly *et al.* (1998) report a detection of modes with  $\ell$  up to 20 in  $\tau$  Peg. Photometry alone may yield only circumstantial evidences. For instance peaks at frequencies above the instability range for p-modes could be interpreted as being due to high- $\ell$  f-modes if they cannot be accounted for in

terms of nonlinear effects of lower frequency modes. This was the argument made by Daszyńska-Daszkiewicz *et al.* (2006) regarding the high-frequency peaks in the  $\delta$  Sct star FG Vir. However, we can never be sure that the inventory of the lower frequency peaks is complete.

## 6. Summary and Discussion

The secondary periodicity in the first overtone Cepheids at about 0.6 of the dominant period presents a challenge to stellar pulsation theory. The phenomenon is not rare. Soszyński *et al.* (2010) found it in 8.5% of the SMC 1O Cepheids. The incidence in the LMC is much lower, but still is seen nearly 2.4% of the objects, also the range of period is much narrower. Objects exhibiting such secondary periodicity are called in this paper the 1O/X Cepheids. In the SMC, they form three detached sequences centered around period ratios 0.61, 0.62, and 0.64 in the Petersen diagram. Except for avoiding the shortest periods, there is nothing that distinguishes these objects from the rest of the first overtone Cepheids.

One F/1O/X Cepheid was found in the LMC but the F-mode amplitude is exceptionally low. No object that could be regarded as the F/X Cepheid has yet been found. The phenomenon seems restricted to the first overtone pulsators but not to Cepheids. Olech and Moskalik (2009) found the secondary periodicity in seven RRc stars in  $\omega$  Cen with the period ratios between 0.608 and 0.622. Period ratios in the [0.612, 0.632] range were found in three RRc stars observed with Kepler space telescope (Moskalik *et al.* 2012). Earlier, a peak near  $0.6P_{1O}$  was found in the RRd star AQ Leo by Gruberbauer *et al.* (2007).

Parameters of all 1O/X Cepheids in the Magellanic Clouds are well constrained by Wesenheit index. Results of linear nonadiabatic calculations for envelope models consistent with observed parameters seem to exclude interpretation of the secondary periodicity in terms of a higher radial overtone. The closest period is that of the third overtone but, in most cases, it is far too long. In remaining cases the third overtone is stable. It is unstable only at the shortest 1O periods, where the period ratio discrepancy is the greatest. It is very difficult to imagine modification in stellar models that could save the interpretation of the 1O/X Cepheids as double radial mode pulsators.

A possibility that the secondary periodicity is due to a nonradial mode trapped in the envelope was considered in Section 3. The conclusion was that only high-degree f-modes remain unstable at the puzzling high frequencies. The instability of such modes over wide ranges of frequencies and stellar parameters has been known for years but has never been satisfactorily explained. In Section 4, we could see that the crucial role in the instability is played by the horizontal radiative transport, which results in energy gain (loss) of the gas element in the high (low) temperature phase. Nothing is known about nonlinear development of the instability

The three sequences of the SMC 1O/X Cepheids corresponding to  $P_X/P_{1O} \approx 0.64, 0.62,$  and  $0.61$  may be associated with single angular degrees  $\ell = 42, 46,$  and

50, respectively. It is not surprising that the degrees are even because amplitude reduction caused by cancellation effect is stronger at odd  $\ell$ 's. No explanation was given why the selected values are multiples of four. In fact, the greatest difficulty of this interpretation are large values of  $\ell$ 's. Typical amplitudes of variability in the  $I$ -band at the puzzling frequencies are in the 4–10 mmag range. To reach such an amplitude against the cancellation effect we must postulate the rms-values of  $\delta R/R$  similar to that of the radial first overtone. Excitation of a high- $\ell$  mode with so large amplitude would manifests itself in a nearly constant, large (35–70 km/s) spectral line broadening. No spectroscopic data are available for any Cepheid known as a 1O/X object. However, overlooking the low amplitude signal is more likely than the predicted large line broadening. Still, even if the explanation in terms of f-modes looks unrealistic, spectroscopic observations of the 1O/X Cepheids are most desired because data on line profiles may yield a clue to the correct explanation.

**Acknowledgements.** I am grateful to Paweł Moskalik for his helpful remarks after reading preliminary version of this paper.

## REFERENCES

- Claret, A. 2000, *A&A*, **363**, 1081.  
 Daszyńska-Daszkiewicz, J. Dziembowski, W.A., and Pamyatnykh, A.A. 2006, *Mem. Astron. Soc. Italiana*, **77**, 113.  
 Dziembowski, W. 1977, *Acta Astron.*, **27**, 95.  
 Dziembowski, W.A., and Smolec, R. 2009, *AIP Conf. Ser.*, **1170**, 83.  
 Feuchtinger, M., Buchler, J.R., and Kolláth, Z. 2000, *ApJ*, **544**, 1056.  
 Girardi, L., Bressan, A., Bertelli, G., and Chiosi, C. 2000, *A&AS*, **141**, 371.  
 Gruberbauer, M., *et al.* 2007, *MNRAS*, **379**, 1498.  
 Kennelly, E.J., *et al.* 1998, *ApJ*, **495**, 440.  
 Kovtyukh, V.V., Andrievsky, S.M., Luck, R.E., and Gorlova, N.I. 2003, *A&A*, **401**, 661.  
 Kurucz, R. L. 2004, <http://kurucz.harvard.edu>.  
 Moskalik, P., and Dziembowski, W.A. 2005, *A&A*, **434**, 1077.  
 Moskalik, P., and Kołaczkowski, Z. 2008, *Comm. in Asteroseismology*, **157**, 343.  
 Moskalik, P., and Kołaczkowski, Z. 2009, *MNRAS*, **394**, 1649.  
 Moskalik, P., *et al.* 2012, ArXiv:1208.4251v1.  
 Mulet-Marquis, C., Glatzel, W., Baraffe, I., and Winisdoerffer, C. 2007, *A&A*, **465**, 937.  
 Olech, A., and Moskalik, P. 2009, *A&A*, **494**, L17.  
 Osaki, Y. 1977, *PASJ*, **29**, 235.  
 Paxton, B., Bildsten, L., Dotter, A., Herwig, F., Lesaffre, P., and Timmes, F. 2011, *ApJS*, **192**, 3.  
 Petersen, J.O. 1973, *A&A*, **27**, 89.  
 Pietrinferni, A., Cassisi, S., Salaris, M., and Castelli, F. 2006, *ApJ*, **642**, 797.  
 Shibahashi, H., and Osaki, Y. 1981, *Publ. Astron. Soc. Japan*, **33**, 427.  
 Soszyński, I., Poleski, R., Udalski, A., Kubiak, M., Szymański, M., Pietrzyński, I., Wyrzykowski, Ł., Szewczyk, O., and Ulaczyk, K. 2008, *Acta Astron.*, **58**, 163.  
 Soszyński, I., Poleski, R., Udalski, A., Kubiak, M., Szymański, M., Pietrzyński, I., Wyrzykowski, Ł., Szewczyk, O., and Ulaczyk, K. 2010, *Acta Astron.*, **60**, 17.  
 Souffrin, P., and Spiegel, E.A. 1967, *Annal. d'Astroph.*, **30**, 985.  
 Stellingwerf, R.F. 1978, *AJ*, **83**, 1184.  
 Townsend, R.H. 2003, *MNRAS*, **343**, 125.